Oral Presentation

The 7th TSME International Conference on Mechanical Engineerin
13-16 December 201

TSME ICOME 2016
Mechanical Engineering Innovation for Green Society

TSF0016

Structures, Jet-and-Crossflow Interactions, and Cross-Plane Entrainment Mechanisms of Jet and Controlled Jet in Crossflow

Intakarn Na Takuathung, and Asi Bunyajitradulya*

Department of Mechanical Engineering, Faculty of Engineering, Chulalongkorn University,
Bangkok 10330, Thailand
* Corresponding Author: E-mail: asi.b@chula.ac.th, Telephone Number: +662 218 6645, Fax Number: +662 218 6645

Abstract

Structures, jet-and-crossflow interactions, and cross-plane entrainment mechanisms of jet and controlled jet in crossflow (JICF and cJICF) at high jet-to-crossflow effective velocity ratio r of 12 are investigated. The results are then compared to JICF at lower r of 4 as reported by Sornphrom and Bunyajitradulya (2016). On the one hand, in order to determine the volumetric entrainment ratio (E) more directly, velocity field information from Stereoscopic Particle Image Velocimetry (SPIV) with (A) jet-fluid only seeding scheme is required. On the other hand, in order to investigate the jet-fluid mixture structures, jet-and-crossflow interactions, and consequently the entrainment mechanisms, additional velocity field information from SPIV with (B) both jet and crossflow fluids seeding scheme is required. As a result, (C) the pure crossflow fluid property can be approximated from the scheme $C = B - A$, employed earlier by Sornphrom and Bunyajitradulya (2016). The experiment is conducted for a baseline JICF at r of 12; crossflow Reynolds number (Re_{cf}) of 3,100; jet Reynolds number of (Re_{j}) of 37,000; the jet initial velocity profile of fully-developed turbulent pipe flow. In the cJICF case, case I165, a pair of azimuthal control jets is injected steadily and radially into the main jet before the jet exit at the azimuthal position ($\pm\theta$) of $\pm 165°$ and the control jets to main jet mass flow rate ratio (r_m) of 4%. The present results show the followings. I) The injection of the control jets at $\theta = \pm 165^{o}$ helps enhancing entrainment over JICF, consistent with earlier result by Wangkiat *et al.* (2015). II) When compared to JICF at lower r of 4, similar five flow features are observed in both the present cases of JICF and I165. In addition, similar cross-plane entrainment mechanism is also observed: namely, 1) Jet-CVP-induced surrounding pure crossflow vortical motion, 2) Jet-CVP-induced vertical channel of high upward flow, and 3) Free-jet like entrainment of jet kidney-shaped structure. However, some differences can also be identified. III) When compared JICF at higher r of 12 to that at lower r of 4, it is found that the region of relatively intense entrainment at higher r occurs earlier during the sequence of downward-inward motion of the jet-CVP-induced pure crossflow vortical motion while that at lower r occurs later during the sequence of inward-upturn motion. This results in the region of intense entrainment of JICF at higher r being located more towards the high-lateral side of the jet than that of lower r, which is located more towards the bottom-center of the jet, i.e., in the converging section of the vertical channel of high upward flow. IV) On the other hand, when compared JICF and I165 at this higher r of 12, it is found that while the region of intense entrainment of JICF is mainly in the lateral-lower half of the jet, that of I165 spans in both the lateral-lower and -upper halves of the jet.

Keywords: Jet in crossflow, entrainment, mechanism, counter-rotating vortex pair (CVP), control jets

1. Introduction

A jet in crossflow (JICF), or transverse jet, is a flow in which a jet is injected normally into a crossflow. As the jet encounters the crossflow, it interacts with the crossflow, resulting in various vortical structures such as jet shear layers, horseshoe vortices, wake vortices, and counter-rotating vortex pair (CVP) (Fric and Roshko, 1994). These jet-and-crossflow interaction and flow structures in turn govern various jet characteristics such as jet trajectory, circulation, and entrainment. These jet characteristics also in turn affect its effectiveness in uses in many engineering applications such as fuel/dilute-air injection in combustion chamber, smoke stack, Vertical Short Take Off and Landing (V/STOL), and film cooling on turbine blade.

In this regard, our researches on JICF have been on various related aspects, the three of which lead us to the present work. They can be outlined as follows.

1. Due to the importance of the manipulation and control of JICF trajectory and entrainment in various applications, especially to promote entrainment and mixing, we have developed a flow control technique, namely *azimuthal control jets*, so that JICF trajectory and, especially, entrainment can be (actively) manipulated, controlled, and promoted (Kornsri *et al.*, 2009; Wangkiat *et al.*, 2015; Tekhuad and Bunyajitradulya, 2016; see also, Tekhuad, 2015).

In this regard, Tekhuad and Bunyajitradulya (2016) have shown that, for JICF at the effective velocity ratio r of 4, windward deployment of a pair of steady azimuthal control jets suppresses entrainment while leeward deployment promotes entrainment,

when compared to the baseline JICF. Furthermore, they also find that the entrainment of controlled jet in crossflow (cJICF) continuously increases as the azimuthal positions of the pair $\pm\theta$, measured from the windward side, increases from windward to leeward, with the two extreme positions $\pm 15^o$ (case I15) and $\pm 165^o$ (case I165) give the lowest and highest accumulative time-mean volumetric entrainment ratio E, respectively. Note that their resolution of the azimuthal positions of the control jets is 15^o.

2. Due to rare data on JICF entrainment owing to the difficulty in determining entrainment experimentally and more directly and due to the desire to evaluate the effectiveness of the use of the azimuthal control jets developed in (1) in manipulating and controlling JICF entrainment, we have developed a technique to measure entrainment more directly using Stereoscopic Particle Image Velocimetry (SPIV) together with the jet-fluid only seeding scheme (Witayaprapakorn and Bunyajitradulya, 2013; Chaikasetsin *et al*., 2014; Bunyajitradulya, 2015). Furthermore, not only that this technique allows us to determine entrainment experimentally and more directly, but also it gives us information on the probability of finding jet-fluid mixture, and the jet-fluid mixture structures and the associated jet-fluid mixture properties and characteristics.

In this regard, this technique has been employed in our past works as referenced. Nonetheless, on the one hand, this technique is still in its early stage and need further refinement; on the other hand, overall it gives consistent results in various aspects with past works. Examples are on entrainment, it gives consistent result on the volumetric entrainment ratio E with that of Yuan and Street (1998); on jet circulation, scaling law, and decay, with that of Broadwell and Breidenthal (1984); on jet trajectory, with conventional power-law trajectory reported by many past works. Some of these aspects are reported in the companion paper by Pruekwatana and Bunyajitradulya (2016).

3. Due to the importance of basic data, knowledge, and understanding in flow structures, jet-and-crossflow interactions, and entrainment mechanism in further advancing the flow control techniques, we have developed an experimental technique and data analysis scheme based on SPIV with both seeding schemes: (A) jet-fluid only seeding and (B) jet-and-crossflow fluids, or both-fluids, seeding in order to extract (C) pure crossflow properties. We shall refer to this technique simply as technique $C = B - A$. More importantly, with this technique we can extract information on the probabilities of finding jet-fluid mixture and of pure crossflow fluid, the jet-fluid mixture structures and the associated jet-fluid mixture properties and characteristics, the jet-and-crossflow interactions, the jet-induced pure crossflow motion, the jet entrainment mechanism, and the distribution of jet entrainment rate and the region of high entrainment rate (Sornphrom and Bunyajitradulya, 2016; see also Sornphrom, 2015; Soupramongkol, 2015).

In this regard, Sornphrom and Bunyajitradulya (2016), hereafter referred to as SB (see also Sornphrom, 2015; Soupramongkol, 2015), have used the technique $C = B - A$ to investigate the jet-fluid mixture structures, the jet-and-crossflow interactions, the jet-induced pure crossflow motion, and the cross-plane entrainment mechanism of JICF at the effective velocity ratio r of 4 and found that cross-plane entrainment mechanism of JICF can be summarized in three subsequent stages. 1) Jet-CVP-induced pure crossflow vortical motion: In this stage, pure crossflow fluid from each lateral side of the jet is induced to have downward-inward-and-upturn motion towards the bell-shaped inlet of the converging-diverging vertical channel of high upward flow at the bottom edge of the jet. 2) Jet-CVP-induced converging-diverging (C-D) vertical channel of high upward flow: The induced pure crossflow fluid at the bottom edge of the jet below and around the bell-shaped inlet is subsequently induced upwards and into the C-D vertical channel of high upward flow. As the pure crossflow fluid is going through the converging section of the channel, it is entrained continuously but intensely in the upstream portion of the converging section of the channel. The intensity and the rate of entrainment in the upstream portion of the converging section is such that, when the fluid reaches the throat of the channel at the center of the gulf region of the jet kidney-shaped structure, it already becomes mostly jet-fluid mixture. 3) Free-jet like entrainment by the jet kidney-shaped structure: The jet-fluid mixture in the gulf region of low streamwise velocity is further entrained into the jet kidney-shaped structure of high streamwise jet velocity, similar to free-jet entrainment.

With the developments in our past works, in this work we attempt to use the experimental technique and scheme $C = B - A$ developed in (3) in order to gain further insight into the entrainment mechanism of the controlled jet in crossflow, controlled by using the azimuthal control jets developed in (1). The specific case of interest is case I165, which has been shown previously using the SPIV and jet-fluid only seeding technique developed in (2) to have higher entrainment than the baseline JICF. In the present work, we shall however investigate JICF and cJICF of higher r of 12.

In this regard, review on entrainment mechanisms of JICF is in order. Yuan *et al*. (1999) used LES to study a round jet in crossflow and found that the interaction between upstream and downstream spanwise rollers in the jet bending region creates, at upstream edge of the jet, a large gap into which incoming crossflow fluid is engulfed. In addition, as for the role of the CVP, they also found that the mean circulation of the CVP helps increasing the surface area of the jet, which results in entrainment

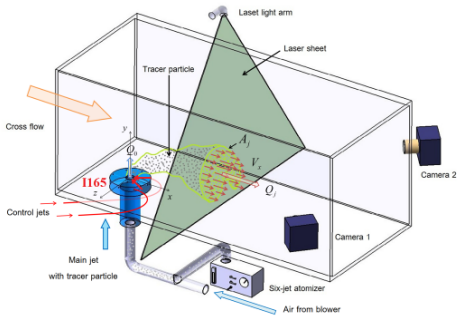

Fig. 1. Experimental setup (Chaikasetsin *et al.*, 2014)

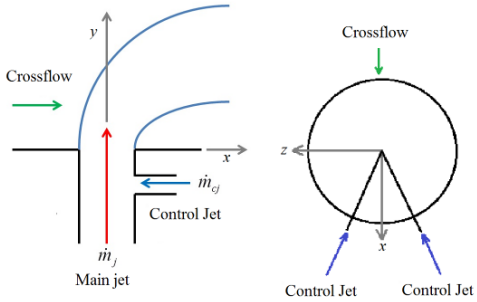

Fig. 2. Schematic of azimuthal control jets.

enhancement. Cortelezzi and Karagozian (2001) simulated JICF using three-dimensional vortex element method and found that JICF entrainment is due to the incoming upstream crossflow near the wall being deflected about the jet, and lifted up on the lee side and into the center region between the CVP. Subsequently, it is wound and entrained into the CVP. Sau *et al*. (2004) simulated a square jet in crossflow and found that both the tails of the upstream horseshoe vortical structures and the surrounding incoming floor shear layer outside the horseshoe vortex system are lifted up from the floor on the lee side of the jet and subsequently entrained into the CVP.

2. Experimental Setup and Condition, Experimental Principles and Techniques

2.1. Experimental setup

The experimental setup for the present work is shown in Fig. 1 (Chaikasetsin *et al.*, 2014); it is the same setup used in SB. Briefly, the setup consists of three main parts: 1) a 50 × 50 cm^2 test-section open-circuit blower-type wind tunnel that is used to generate uniform crossflow, 2) the 12.57 mm inner diameter (d) main jet system that is used to generate the main jet with full-developed turbulent pipe flow velocity profile at the jet exit; this is achieved by having a straight pipe section of $77d$ long before the jet exit; 3) the control jet systems that is used to generate the azimuthal control jets. Note that the main jet exit and the control jets are integrated as one assembly as shown in Fig. 2. For the azimuthal control jets, a total of 24 azimuthal control jets with inner diameter (d_{cj}) of 0.5 mm are aligned radially (injected radially into the main jet) and spaced azimuthally around the main jet exit at a uniform spacing of 15^o; these control jets are located, and the control jets injected, at 3 mm below the main jet exit plane.

The coordinate system employed in this work is right-handed Cartesian as shown in Fig. 1, where x is streamwise (in the direction of the crossflow), y is transverse (in the direction of the main jet at the jet exit), and z is spanwise (according to right-handed system). Note that we shall use $\vec{x}$ as a position vector from the origin, which is located at the center of the main jet at the jet exit plane, while x is simply the streamwise coordinate: $\vec{x} = (x, y, z)$.

2.2. Experimental condition

The experiment is conducted for a baseline JICF with the effective velocity ratio r of 12. The effective velocity ratio r is defined as the square root of the jet-to-crossflow momentum flux ratio: $r = \sqrt{\rho_j u_j^2 / \rho_{cf} u_{cf}^2}$, where ρ is density, u velocity, and subscripts j and cf refer to the main jet and the crossflow, respectively. For equal density flow such as in this case, the effective velocity ratio r is reduced to the velocity ratio $r_u = u_j / u_{cf}$. For u_j, an area-averaged velocity at the jet exit is used and is equal to 48.4 m/s while the crossflow velocity is uniform at 4.03 m/s. Other flow conditions are no buoyancy effect ($\rho_j / \rho_{cf} = 1$); the crossflow Reynolds number ($\mathrm{Re}_{cf} = u_{cf} d / \nu_{cf}$) is 3,100; the jet Reynolds number ($\mathrm{Re}_j = u_j d / \nu_j = r \times \mathrm{Re}_{cf}$) is 37,200; the initial jet velocity profile measured at the jet exit when the crossflow is turned off is fully-developed turbulent pipe flow; the incoming crossflow boundary layer is laminar, approximately Blasius profile with normalized thickness measured at $x/d = -7$ of $\delta/d \approx 0.6$.

In the case of cJICF, case I165 is experimented, i.e., a pair of steady control jets is activated at $\pm\theta = \pm 165^o$ with the control jets to main jet mass flowrate ratio ($r_m = \dot{m}_{cj} / \dot{m}_j$) of 4%. Note that $\dot{m}_{cj}$ is the total mass flowrate of the two control jets deployed, i.e., each control jet issues r_m of 2%.

Planar velocity fields are measured at 4 cross planes located at x/rd = 0.25, 0.5, 0.75, and 1.0.

2.3. Experimental principles and techniques

The experimental principles and techniques are the same as described in SB. Briefly, the planar velocity fields are acquired in the cross planes located at x with Stereoscopic Particle Image Velocimetry (SPIV) with two PIV tracer particle seeding schemes:

(A) jet-fluid only seeding,
(B) jet-and-crossflow fluids (or both-fluids) seeding.

(A) The first seeding scheme (A) allows us to determine the instantaneous and subsequently the time-mean *jet-fluid mixture velocity*, denoted by $\vec{V}_j = (V_{j,x}, V_{j,y}, V_{j,z})$, in a cross plane at x; the instantaneous and subsequently the time mean *jet-fluid mixture volume flowrate*, denoted by $Q_j(x)$, through the cross plane at x; and finally the *accumulative time-mean jet volumetric entrainment ratio* $E(x) = Q_j(x)/Q_o$, where Q_o is the total volume flowrate of the main jet at the main jet exit. Note that Q_o also includes the volume flowrate of the two control jets in the case of cJICF.

Besides the jet-fluid mixture velocities, volume flowrates, and entrainment, this seeding scheme (A) also allows us to extract information on the probability of finding jet-fluid mixture (ϕ_j), and the jet-fluid mixture structures and the associated properties and characteristics such as jet-fluid mixture trajectory, vorticity, and circulation.

The probability of finding jet-fluid mixture ϕ_j at any spatial point $\vec{x}$ can be found from the ratio of the total snapshots N_j in which SPIV acquired *a* velocity (or non-absolute-zero velocity, which implies that PIV tracer particles can be found at $\vec{x}$, which further implies that there is jet fluid at $\vec{x}$) to the total snapshots N acquired over the data collection period, $\phi_j = N_j / N$. Since at a spatial-time point, SPIV registers either a velocity (jet-fluid mixture is found) or absolute zero velocity (pure crossflow fluid is found), exclusive, $N = N_j + N_{cf}$, where N_{cf} is the total number of snapshots that only pure crossflow fluid is found at the point $\vec{x}$. Therefore, the probability of finding pure crossflow fluid $\phi_{cf} = N_{cf} / N$ at $\vec{x}$ is complementary to the probability of finding jet-fluid mixture ϕ_j at $\vec{x}$, $\phi_j + \phi_{cf} = 1$. Nonetheless, in this work we find and report ϕ_{cf} from C(ϕ_{cf}) = B (ϕ) - A(ϕ_j), where ϕ is the probability of finding any fluid – jet-fluid mixture or pure crossflow fluid - from SPIV with seeding technique B. As will be shown, the seeding in case (B) is fairly steady and uniform such that $\phi \approx 1$ over a cross section.

(B) On the other hand, for the seeding scheme (B), in which both jet and crossflow fluids are seeded with PIV tracer particles, we cannot differentiate whether the velocity acquired at that spatial-time point is the velocity of the jet-fluid mixture or the velocity of pure crossflow fluid. This scheme therefore allows us to determine the instantaneous and subsequently the time-mean *field velocity,* denoted by $\vec{V} = (V_x, V_y, V_z)$, in a cross plane at x. This velocity field, however, when compared to the jet-fluid mixture velocity field from (A), is modulated by the surrounding pure crossflow velocity field. Similarly, properties derived from this velocity field such as trajectory, vorticity, and circulation, are not purely jet-fluid mixture properties; they are jet-fluid mixtures properties modulated by the surrounding pure crossflow property.

(C) Subsequently, for a steady-in-mean flow, if we subtract the time-mean jet-fluid mixture velocity $\vec{V}_j$, derived from (A) from one realization, from the time-mean field velocity $\vec{V}$, derived from (B) from another realization, we have the approximate of the time-mean *pure crossflow velocity*:

C = B – A : $\vec{V}_{cf} = (V_{cf,x}, V_{cf,y}, V_{cf,z}) \approx \vec{V} - \vec{V}_j$.

Similar statement C = B – A can be applied and stated for other properties such as vorticity:

C = B – A : pure crossflow property
= field property – jet property

Further details in this regard can be found in SB.

Finally, for clarity, in this work we shall refer to the velocity derived from SPIV and seeding scheme (A) as the *jet-fluid mixture velocity* or simply as the *jet velocity*, denoted by $\vec{V}_j$. Accordingly, we shall refer to any property derived from it as the *jet-fluid mixture property* or simply as *jet property*. We shall use the subscript ' j ' with notations for such properties, q_j. This is to contrast to the velocity field derived from SPIV and seeding scheme (B), in which there is no differentiation whether the velocity at that spatial-time point belongs to the jet-fluid mixture or to the surrounding pure crossflow. As such, it is the modulation of the jet-fluid mixture velocity field and the surrounding pure crossflow velocity field. We shall refer to the velocity field acquired with SPIV with seeding scheme (B) as the *field velocity*, denoted by $\vec{V}$, and we shall refer to any property derived from it as the *field property*, denoted simply by q, where no subscript is used with such properties. Lastly, we shall refer to the velocity field derived from C = B – A as the *pure crossflow velocity*, denoted by $\vec{V}_{cf}$, and we shall refer to any property derived from it as the *pure crossflow property*. We shall use the subscript ' *cf* ' with notations for such properties, q_{cf}.

Finally, in this work the PIV tracer particles used are glycerol solution 5% by volume for jet-fluid seeding (in both schemes A and B) and 50% by volume for crossflow-fluid seeding (in scheme B). The planar velocity field data for all cases are collected at 2.07 Hz and for a total of 1,000 snapshots, or 1,000 instantaneous velocity fields.

3. Results

3.1. Volumetric entrainment ratio, E

Figure 3 shows the developments of the accumulative time-mean volumetric entrainment ratio

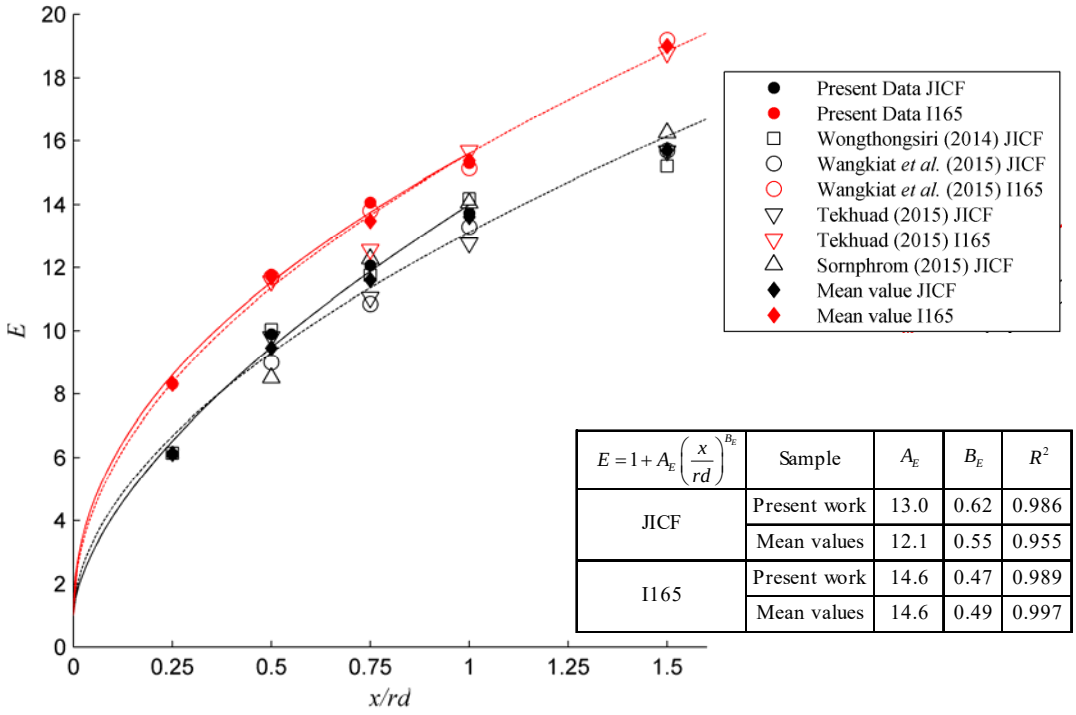

$E=1+A_E\left(\frac{x}{rd}\right)^{B_E}$	Sample	A_E	B_E	R^2
JICF	Present work	13.0	0.62	0.986
	Mean values	12.1	0.55	0.955
I165	Present work	14.6	0.47	0.989
	Mean values	14.6	0.49	0.997

Fig. 3. Development of entrainment along x/rd in JICF and I165. Model fits are through the present data (solid lines) and the mean values of all data at each plane (dashed lines).

along the streamwise direction on rd-scale, $E(x/rd)$, for the present data and the past data of our group. For both cases of JICF and I165, it is found that entrainment naturally increases as the jet develops downstream. As a steady pair of control jets are applied in I165, entrainment increases over that of JICF for all planes experimented. In addition, the one-plus-power law: $E=1+A_E(x/rd)^{B_E}$, can reasonably well represent experimental data; the coefficients of the model fits are given in the table in the figure. Note that we fit two lines for each case: the solid line is the fit through the present data while the dashed line is the fit through the mean value (including the present data in the sample) of each plane. In order to give some indication of the scatter of our data, the mean-normalized standard deviation in per cent, S_E/E (×100%), is calculated. It is found that the scatter of data measured with S_E/E for all x/rd stations for JICF is less than 7.1% with the mean 3.9% and for I165 is less than 6.0% with the mean 2.6%.

3.2. Structures, jet-and-crossflow interactions, and cross-plane entrainment mechanism

Analysis and scheme for presenting the results

For the analysis and scheme for presenting the results in Figs. 4 and 5, we take the same approach as reported in SB. Briefly, we take the C = B – A scheme and presented

(A) q_j, the jet-fluid mixture property,

(B) q, the field property,

(C) q_{cf}, the pure crossflow property,

as sub-plots (A), (B), and (C) in Figs. 4 and 5. Note that all quantities presented are time-mean quantities.

- **Contour surfaces**

  For contour surfaces, we presented
  - the probabilities: $A=\phi_j$, $B=\phi(\approx 1)$, $C=\phi_{cf}$,
  - the u_{cf}-normalized time-mean streamwise velocities: $A=V_{j,x}/u_{cf}$, $B=V_x/u_{cf}$, $C=V_{cf,x}/u_{cf}$
  - the u_{cf}/d-normalized time-mean streamwise vorticities: $A=\omega_{j,x}d/u_{cf}$, $B=\omega_x d/u_{cf}$, $C=\omega_{cf,x}d/u_{cf}$.

- **Contour lines**

  Selected contour lines of the probability of finding jet-fluid mixture ϕ_j are superimposed on all sub-plots of Figs. 4 and 5 for reference to different regions over the jet cross section. The selected values of ϕ_j are, from outer to inner, 0.01, 0.25, 0.75, 0.95. The reason for these values can be found in Bunyajitradulya

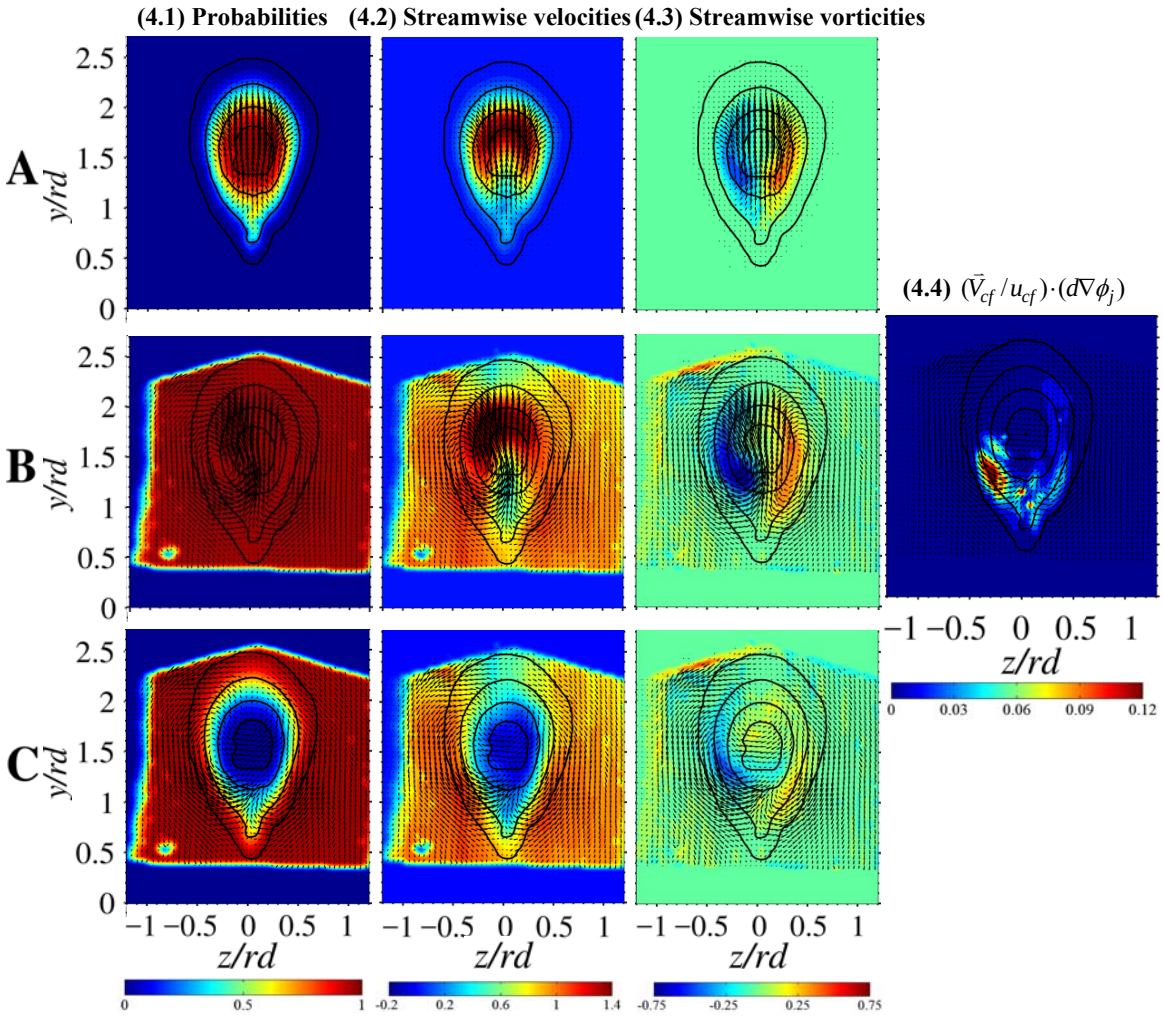

Fig. 4. JICF: Normalized time-mean property fields at $x/rd = 0.75$.
Surface contours: (4.1) probabilities, (4.2) streamwise velocities, (4.3) streamwise vorticities, and (4.4) $(\vec{V}_{cf}/u_{cf})\cdot(d\nabla\phi_j)$.
In-plane vectors: Normalized time-mean in-plane velocity fields.
Contour lines: from outer to inner, $\phi_j = 0.01$, 0.25, 0.75 and 0.95.

(2015). Briefly, they are lines that differentiate different regions of the jet-fluid mixture cross section according to their contribution to the total time-mean jet area: being linear in the approximated range of $0 < \phi_j / \phi_{j,\max} < 0.01$ and $0.25 < \phi_j / \phi_{j,\max} < 0.75$, where $\phi_{j,\max}$ is the maximum ϕ_j at that cross section, which is typically close to one in the range of parameters investigated.

In this regard, all sub-plots (A)-(C) of the same flow (JICF or I165) have the same contour lines.

- **In-plane vector**

Furthermore, the u_{cf} -normalized time-mean in-plane velocity field is also superimposed on the corresponding plot. In this case, (A) is the jet velocity, $\vec{V}_{j,yz}/u_{cf}$, (B) is the field velocity, $\vec{V}_{yz}/u_{cf}$, and (C) is the pure crossflow velocity, $\vec{V}_{cf,yz}/u_{cf}$.

3.2.1. JICF

Figure 4 shows the result for JICF at the cross plane $x/rd = 0.75$. In this figure, contour surfaces are for (4.1) the probabilities, (4.2) the time-mean

streamwise velocities, (4.3) the time-mean streamwise vorticities, and (4.4) $(\vec{V}_{cf,yz}/u_{cf})\cdot(d\nabla\phi_j)$, which is indicative of the local pure crossflow volume flowrate that is 'disappeared' (from the cross plane) down the gradient of the probability of finding pure crossflow fluid $(-\nabla\phi_{cf}=\nabla\phi_j)$, or up the gradient of finding the jet-fluid mixture, per unit volume.

Overall, the structures, jet-and-crossflow interactions, and entrainment mechanism are similar to JICF at $r=4$ as reported by SB. Nonetheless, there are some differences that we can observe.

For the probabilities (Fig. 4.1), it is found that at the center of the jet the probability of finding the jet fluid ϕ_j is high while the probability of finding the pure crossflow fluid ϕ_{cf} is low. As we move towards the jet edge, ϕ_j decreases towards zero while naturally ϕ_{cf} increases towards one. Note that on the average while ϕ_{cf} is a measure of the probability, $-\nabla\phi_{cf}=\nabla\phi_j$ is indicative of the spatial rate at which pure crossflow fluid disappears (from the cross plane), part of which is due to entrainment by the jet (and part of which is due to out-of-plane flow).

When we compare the probability of finding jet-fluid mixture ϕ_j in this case of JICF at higher r of 12 to that of SB at lower r of 4, it is interesting to note that, at the same $x/rd=0.75$ cross plane, JICF at this higher r of 12 has lower maximum value of ϕ_j than JICF with lower r of 4; being less than 0.99 when compared to more than 0.99. This indicates that JICF at higher r is less steady, with more meandering, than JICF at lower r.

For the normalized time-mean in-plane velocities (Fig. 4.1), it is found that the contribution to the typical vortical motion associated with the counter-rotating vortex pair (CVP) observed in past studies as well as in Fig. 4.1B consists of two 'halves.' The first half, which is contributed by the jet-fluid mixture due to the jet CVP, is evident in Fig. 4.1A. Note that the jet CVP itself can be identified more clearly from the time-mean streamwise jet vorticity (Fig. 4.3A). The second half, which is due to the surrounding pure crossflow fluid being induced by the jet CVP to participate in its vortical motion, is evident in Fig. 4.1C. For this, the pure crossflow fluid on each lateral side of the jet is induced to have downward-inward-and-upturn motion, from each lateral side of the jet towards the bottom edge of the jet. During the process of moving inward and upturn, the pure crossflow fluid is moving down the gradient of the probability of finding the pure crossflow fluid $(-\nabla\phi_{cf})$, or up the gradient of the probability of finding the jet-fluid mixture $(+\nabla\phi_j)$. In other words, the pure crossflow fluid is partly being entrained into the jet. After this, the fluid is further induced to have an upward motion through the converging-diverging vertical channel of high upward flow (Fig. 4.1B), which is located at the center and in between the vortex pair of the jet CVP and whose existence is also induced and fueled by the jet CVP. Compared to JICF at lower r of SB, the vertical channel of high upward flow in the present case of higher r is less symmetric.

As found in SB for JICF at $r=4$ and here at $r=12$, from the time-mean in-plane velocity fields (together with the streamwise jet vorticity field) we can identify three important features of the flow: 1) the jet CVP (Figs. 4.1A, 4.3A), 2) the jet-CVP-induced surrounding pure crossflow vortical motion (Fig. 4.1C), and 3) the jet-CVP-induced converging-diverging vertical channel of high upward flow (Fig. 4.1B). These features play important role in JICF cross-plane entrainment, albeit maybe at different degrees than JICF at lower r.

For the normalized time-mean streamwise velocities (Fig. 4.2), similar to SB, we can identify two additional features of the flow from the streamwise jet velocity $V_{j,x}/u_{cf}$ (Fig. 4.2A): 4) the jet kidney-shaped (K-S) structure of high streamwise jet velocity, and 5) the gulf region (G-R) of low streamwise jet velocity, which lies underneath the jet kidney-shaped structure. Note that we reference the jet kidney-shaped structure and the gulf region to the jet streamwise velocity. Comparing this to JICF at lower r of 4 of SB, the gulf region of this higher r is shallower, at least at this streamwise location. For the streamwise pure crossflow velocity $V_{cf,x}/u_{cf}$ (Fig. 4.2C), at the center of the jet the pure crossflow also has relatively low streamwise velocity.

For the u_{cf}/d -normalized time-mean streamwise vorticities (Fig. 4.3), the dominant jet counter-rotating vortex pair, referred to as the *jet CVP*, is evident (Fig. 4.3A). The vortex pair has inward-facing, inverse comma shape with high vorticity at the heads of the commas. In addition, a pair of pure crossflow counter-rotating vortex pair near the heads of the commas at the lateral-bottom side of the jet CVP is also observed (Fig. 4.3C). This vortex pair is of the same sign as the jet CVP. This pure crossflow CVP is most likely associated with the crossflow boundary layer that is lifted up at the lee side of the jet as wake vortices system.

As for cross-plane JICF entrainment mechanism, it is found that the entrainment mechanism is, to some degree, similar to the case of JICF at lower r of 4 of SB (see also Sornphrom, 2015; Soupramongkol, 2015). Specifically, the jet CVP (Fig. 4.3A) induces the surrounding pure crossflow fluid to participate in its vortical motion (Figs. 4.1C and 4.1B) such that the pure crossflow fluid from each lateral side of the jet has a sequence of downward-inward-and-upturn motion, from each lateral side of the jet towards the bottom side and continuing on into the vertical channel of high upward flow. The difference between the present JICF at higher r of 12 and that at lower r of 4 is that, for JICF at this higher r the region of intense

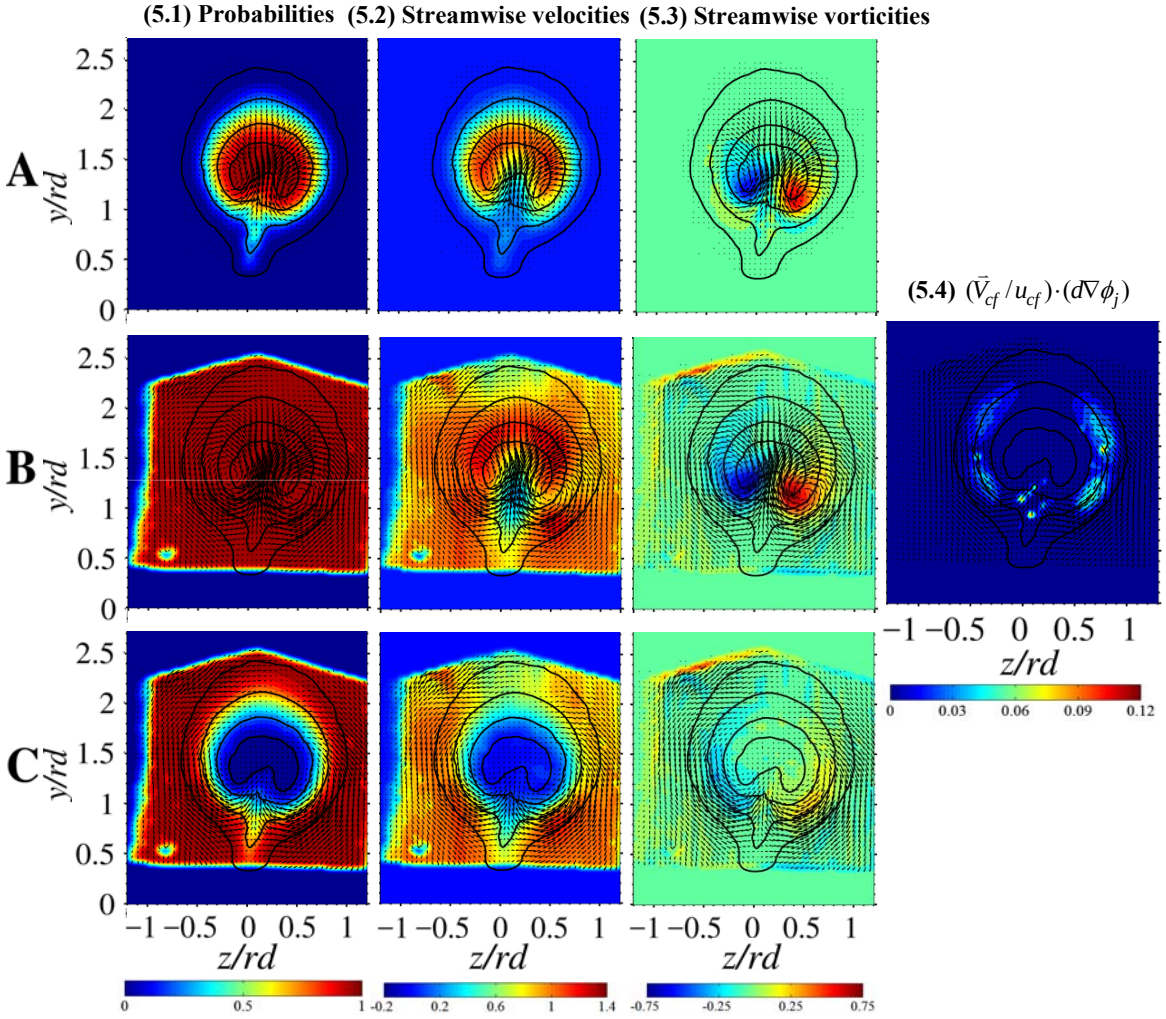

Fig. 5. I165: Normalized time-mean property fields at $x/rd = 0.75$. The plotting scheme is the same as Fig. 4.

entrainment occurs relatively early during the sequence of downward-inward motion of the jet-CVP-induced pure crossflow vortical motion while that for JICF at lower r occurs relatively later during the sequence of inward-upturn motion (i.e., in the converging section of the vertical channel of high upward flow). This results in the region of intense entrainment of JICF at higher r being located more towards the high-lateral side of the jet than that of lower r, which is located more towards the bottom-center of the jet in the converging section of the vertical channel. The local rate of cross-plane entrainment can be inferred from the flow of pure crossflow fluid ($\vec{V}_{cf}$) down the gradient of the probability of finding pure crossflow fluid ($-\nabla\phi_{cf}$), or up the gradient of the probability of finding the jet fluid ($\nabla\phi_j$). The region of intense entrainment can therefore be inferred from the distribution of $(\vec{V}_{cf}/u_{cf})\cdot(d\nabla\phi_j)$ shown in Fig. 4.4.

Similar to JICF at lower r of 4, when the fluid reaches the throat of the converging-diverging vertical channel of high upward flow, it becomes mostly now the jet-fluid mixture, which is further entrained by the jet kidney-shaped structure like free-jet entrainment.

3.2.2. I165

The results for the controlled jet in crossflow I165, which gives higher entrainment than the baseline JICF, are shown in Fig. 5. Overall, similar five flow features as those of JICF are observed: 1) the jet CVP [Fig. 5.3A], 2) the jet-CVP-induced surrounding pure crossflow vortical motion [Figs. C], 3) the jet-CVP-induced vertical channel of high upward flow [Figs. B], 4) the jet kidney-shaped structure of high streamwise jet velocity [Fig. 5.2A], and 4) the gulf

region of low streamwise jet velocity [Fig. 5.2A]. In addition, the two contributions to the typically-observed vortical motion associated with CVP (Figs. B): from the jet-fluid mixture (Figs. A) and from the surrounding pure crossflow fluid (Figs. C), are evident. Of particular note is that while the baseline JICF has the overall shape of inversed teardrop, when the control jets are applied it becomes rounder and more symmetric.

As for the cross-plane entrainment mechanism, overall it is still similar to JICF, i.e., the jet-CVP entrainment dominated. However, while the region of intense entrainment of JICF is mainly in the lateral-lower half of the jet (Fig. 4.4), that of I165 spans both in the lateral-lower and -upper halves of the jet (Fig. 5.4).

4. Discussions

In order to get an overview of entrainment in JICF as well as two unresolved issues that we encounter, some discussions are in order.

Firstly, it needs to be recognized that, unlike concentration, the probability of finding jet-fluid mixture ϕ_j does not take the concentration of jet-fluid mixture into account. The SPIV either register *a* velocity or not, exclusive. Therefore, while ϕ_j can be used as an indirect indicator, it is not a direct measure, of concentration.

Secondly, while we find that the entrainment of I165 is more than JICF, the comparison of $(\vec{V}_{cf}/u_{cf})\cdot(d\nabla\phi_j)$ in Figs. 4.4 for JICF and 5.4 for I165 seemingly, but not yet conclusively, suggests otherwise. That is, at least the local maximum value of $(\vec{V}_{cf}/u_{cf})\cdot(d\nabla\phi_j)$ for JICF is higher than I165.

Thirdly, it needs to be recognized that presently we view only the entrainment mechanism in the cross plane, i.e., the cross-plane entrainment. In this regard, Fig. 6 shows the schematic of entrainment of crossflow fluid through the jet side surface of constant ϕ_j. The total crossflow volume flowrate through this side surface Q_{cf,ϕ_j} can be decomposed into two components, one due to in-plane crossflow velocity $Q_{cf,\phi_j,\vec{V}_{cf,yz}}$ and the other to streamwise crossflow velocity $Q_{cf,\phi_j,\vec{V}_{cf,x}}$. In this regard, past works by Yuan *et al.* (1999) have suggested that $Q_{cf,\phi_j,\vec{V}_{cf,x}}$ can be achieved through mechanism such as a gap created by upstream and downstream spanwise rollers at the upstream edge of the jet.

As a result of these, the question arises in regard to 1) the relative contributions of the cross-plane entrainment by the in-plane crossflow velocity $(\vec{V}_{cf,yz})$ and the streamwise entrainment by the streamwise crossflow velocity $(\vec{V}_{cf,x})$, to the total entrainment of JICF. This question further leads to 2)

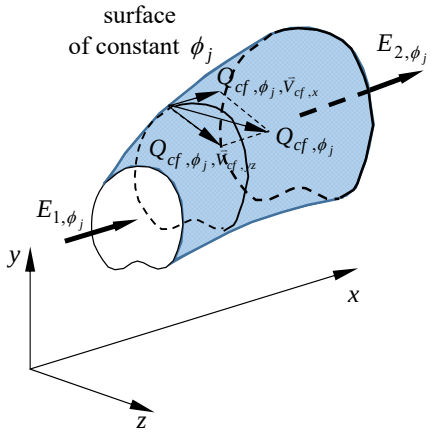

Fig. 6. Entrainment due to crossflow in-plane $(\vec{V}_{cf,yz})$ and streamwise $(\vec{V}_{cf,x})$ velocities.

the question of the use of the azimuthal control jets in I165 as to which mode of entrainment, cross-plane or streamwise, it promotes and through what mechanism. At present, we cannot yet resolve either of these issues, and further investigations are needed.

5. Conclusions

Structures, jet-and-crossflow interactions, and cross-plane entrainment mechanisms of jet and controlled jet in crossflow (JICF and I165) at high effective velocity ratio r of 12 are investigated. The results show that, overall JICF and I165 in the present work of higher r have similar flow features and cross-plane entrainment mechanism as those observed in JICF at lower r of 4 of Sornphrom and Bunyajitradulya (2016). Specifically, five four features that are relevant to cross-plane entrainment are observed: 1) the jet CVP, 2) the jet-CVP-induced surrounding pure crossflow vortical motion, 3) the jet-CVP-induced converging-diverging vertical channel of high upward flow, 4) the jet kidney-shaped structure of high streamwise jet velocity, and 5) the gulf region of low streamwise jet velocity. For cross-plane entrainment mechanism, similar three stages of entrainment are also observed: 1) jet-CVP-induced surrounding pure crossflow vortical motion, 2) jet-CVP-induced vertical channel of high upward flow, and 3) free-jet like entrainment of jet kidney-shaped structure. Nonetheless, some degree of differences among these flows can also be noted as follows.

When we compare JICF at lower r of 4 and higher r of 12, we find that while the region of intense entrainment of JICF at lower r of 4 occurs relatively later during the sequence of inward-upturn motion of the jet-CVP-induced pure crossflow vortical motion, that of higher r of 12 occurs relatively earlier during the sequence of downward-inward motion. This results in the region of intense entrainment of JICF at higher r being located more towards the high-lateral

side of the jet than that of lower r, which is located more towards the bottom-center of the jet, in the converging section of the vertical channel of high upward flow.

When we compare JICF and cJICF (I165) at the same high r of 12, we find that while the region of intense entrainment of JICF is mainly in the lateral-lower half of the jet, that of I165 spans both in the lateral-lower and -upper halves of the jet.

Two issues remain unresolved: one is regarding the relative contributions of the cross-plane entrainment and the streamwise entrainment, to the total entrainment of JICF; the other is regarding as to which mode of entrainment, cross-plane or streamwise, I165 promotes and through what mechanism.

6. Acknowledgements

The first author would like to acknowledge the Bachelor-Master Degree Scholarship, AY 2016, of the Department of Mechanical Engineering, Faculty of Engineering, Chulalongkorn University. We are thankful for suggestions and assistances of Assc. Prof. Vejapong Juttijudata, Mr. Chaowat Tekhuad, Ms. Kwanmon Sornphrom, and Mr. Pattarapol Suppamongkol. We also appreciate the assistances and cooperations of Mr. Sirawit Kuwawattananont and Mr. Aekanut Pruekwatana.

7. References

[1] Broadwell, J. E. and Breidenthal, R. E. (1984). Structure and mixing of a transverse jet in incompressible flow, *J. Fluid Mech.*, Vol. 148, pp. 405-412.

[2] Bunyajitradulya, A. (2015). Evaluation of the volumetric entrainment ratio of a jet in crossflow and its evolution, *Thai Government GRB_APS_23_57_21_01 Research Project Report*, Thai Government Research Fund FY 2557.

[3] Chaikasetsin, S., Sushewakhul, T., Panusittikorn, P., and Bunyajitradulya, A. (2014). Effects of azimuthal control jets to main jet mass flowrate ratio on the entrainment of a jet in crossflow, paper presented in *The Fifth Thai Society of Mechanical Engineers International Conference on Mechanical Engineering* (*TSME-ICoME 5*), December 17-19, 2014, The Empress, Chiang Mai, Thailand. Paper No TSF05.

[4] Cortelezzi, L. and Karagozian, A. R. (2001). On the formation of the counter-rotating vortex pair in traverse jets, *J. Fluid Mech.*, Vol. 446, pp. 347-373.

[5] Fric, T. F. and Roshko, A. (1994). Vortical structure in the wake of a transverse jet, *J. Fluid Mech.*, Vol. 279, pp. 1-47.

[6] Kornsri, P., Pimpin, A., and Bunyajitradulya, A. (2009). A scheme for the manipulation and control of a jet in crossflow: The use of azimuthal control jets, paper presented in *The Twenty-Third Conference of The Mechanical Engineering Network of Thailand* (*ME-NETT 23*), November 4 – 7, 2009, Chiang Mai, Thailand.

[7] Pruekwatana, A. and Bunyajitradulya, A. (2016). Scaling-power law correlations for collapsing the effects of the effective velocity ratio on jet-fluid mixture trajectory, circulation, and entrainment of jets in crossflow, paper presented in *The Seventh Thai Society of Mechanical Engineers International Conference on Mechanical Engineering* (*TSME-ICoME 7*), December 13-16, 2016, Duangtawan Hotel, Chiang Mai, Thailand.

[8] Sau, A., Sheu, T. W. H., Hwang, R. R., and Yang, W. C. (2004). Three-dimensional simulation of square jets in cross-flow, *Phys. Rev. E*, Vol. 69, CID 066302.

[9] Smith, S. H. and Mungal, M. G. (1998). Mixing, structure and scaling of the jet in crossflow, *J. Fluid Mech.*, Vol. 357, pp. 83-122.

[10] Sornphrom, K. (2015). Entrainment and cross-plane entrainment mechanism of jets in crossflow, *Master Thesis*, Department of Mechanical Engineering, Faculty of Engineering, Chulalongkorn University, Bangkok, Thailand. [In Thai]

[11] Sornphrom, K. and Bunyajitradulya, A. (2016). Structures, jet-and-crossflow interactions, and cross-plane entrainment mechanism of a jet in crossflow, paper presented in *The Thirtieth Conference of The Mechanical Engineering Network of Thailand* (*ME-NETT 30*), July 5-8, 2016, Songkhla, Thailand. Paper No. TSF 0015.

[12] Soupramongkol, P. (2015). Effects of azimuthal control jets on entrainment and cross-plane entrainment mechanism of a jet in crossflow, *Master Thesis*, Department of Mechanical Engineering, Faculty of Engineering, Chulalongkorn University, Bangkok, Thailand. [In Thai]

[13] Tekhuad, C. (2015). Optimal injection angles of the azimuthal control jets for entrainment of jets in crossflow, *Master Thesis*, Department of Mechanical Engineering, Faculty of Engineering, Chulalongkorn University, Bangkok, Thailand. [In Thai]

[14] Tekhuad, C. and Bunyajitradulya, A. (2016). Effects of azimuthal position of azimuthal control jets on manipulation and control of entrainment of jets in crossflow, paper presented in *The Thirtieth Conference of The Mechanical Engineering Network of Thailand* (*ME-NETT 30*), July 5-8, 2016, Songkhla, Thailand. Paper No. TSF 0004. [In Thai]

[15] Wangkiat, S., Khemakanon, S., Kengkarnpanich, A., and Bunyajitradulya, A. (2015). Effects of the azimuthal positions of the azimuthal control jets on structures and entrainment of a jet in crossflow at high effective velocity ratio 12, paper presented in *The Sixth Thai Society of Mechanical Engineers International Conference on*

Mechanical Engineering (*TSME-ICoME 6*), December 16-18, 2015, The Regent Cha-am beach Resort, Hua-Hin, Thailand. Paper No TSF006.

[16] Witayaprapakorn, T. and Bunyajitradulya, A. (2013). Effects of azimuthal control jets on structure and entrainment of a jet in crossflow, paper presented in *The Twenty-Seventh Conference of the Mechanical Engineering Network of Thailand* (*ME-NETT 27*), October 16 – 18, 2013, Chonburi, Thailand. [In Thai]

[17] Yuan, L. L. and Street, R. L. (1998). Trajectory and entrainment of a round jet in crossflow, *Phys. Fluids*, vol. 10, no. 9, pp. 2323-2335.

[18] Yuan, L. L., Street, R. L., and Ferziger, J. H. (1999). Large-eddy simulation of a round jet in crossflow, *J. Fluid Mech.*, Vol. 379, pp. 71-104.